# Length Regulation Drives Self-Organization in Filament-Motor Mixtures

Moritz Striebel,[1,*] Fridtjof Brauns,[1,*] and Erwin Frey[1,2,†]
[1]*Arnold Sommerfeld Center for Theoretical Physics and Center for NanoScience, Department of Physics, Ludwig-Maximilians-Universität München, Theresienstrasse 37, D-80333 Munich, Germany*
[2]*Max Planck School Matter to Life, Hofgartenstraße 8, D-80539 Munich, Germany*

(Received 24 August 2021; accepted 10 October 2022; published 30 November 2022)

Cytoskeletal networks form complex intracellular structures. Here we investigate a minimal model for filament-motor mixtures in which motors act as depolymerases and thereby regulate filament length. Combining agent-based simulations and hydrodynamic equations, we show that resource-limited length regulation drives the formation of filament clusters despite the absence of mechanical interactions between filaments. Even though the orientation of individual remains fixed, collective filament orientation emerges in the clusters, aligned orthogonal to their interfaces.

DOI: 10.1103/PhysRevLett.129.238102

The microtubule cytoskeleton plays an important role in numerous cellular functions such as intracellular transport and cell division [1,2]. These complex processes are based on active remodeling of the cytoskeletal structure [3], which is mediated by the interaction of microtubules with a variety of microtubule associated proteins (MAPs) [4–6]. In addition to generating forces between microtubules [7], MAPs play an important role in regulating the length of individual microtubules by affecting the rates of their polymerization kinetics from tubulin subunits [8–11]. How forces affect the large-scale self-organization of microtubules has been studied in detail both theoretically and experimentally [12–18]. In contrast, the role of length regulation has only been investigated in the context of individual filaments [9,19–26], or of a globally accessible pool of constituents (tubulin and MAPs) [27–30]. However, recently the focus of interest is shifting to their role in many filament systems, as there is increasing experimental evidence that this regulatory function, in combination with the local availability of MAPs and tubulin, plays an essential role in the self-organization, scaling and maintenance of microtubule structures [31–37]. It remains an important open question how the interplay and spatial redistribution of these resources through cytosolic diffusion and transport along microtubules affects the self-organization of the microtubule cytoskeleton [38–41].

Here, we approach this question by studying the collective motor-filament dynamics with limited resources of tubulin units and molecular motors. These cytosolic resources are spatially redistributed by diffusion while filament-bound motors additionally move unidirectionally towards the filament plus end where they act as depolymerases (Fig. 1). We show that the interplay of motor-catalyzed depolymerization and local resource availability leads to self-organization of the filament assembly into asterlike patterns. Those patterns show colocalization of microtubule plus ends and polarity sorting at the interfaces of emerging filament clusters.

*Model.*—We propose an agent-based model that builds on current *in vitro* experiments and theoretical studies addressing the resource-limited length regulation of a single stabilized microtubule by the kinesin-8 homologue Kip3 from *Saccharomyces cerevisiae* [26]. Specifically, we study filament dynamics containing a finite number of tubulin units ($N_T$), molecular motors ($N_M$), and filaments ($N_F$); see Fig. 1(b). Each individual filament $i \in 1, \ldots, N_F$ is represented by a directed rigid rod with fixed minus-end

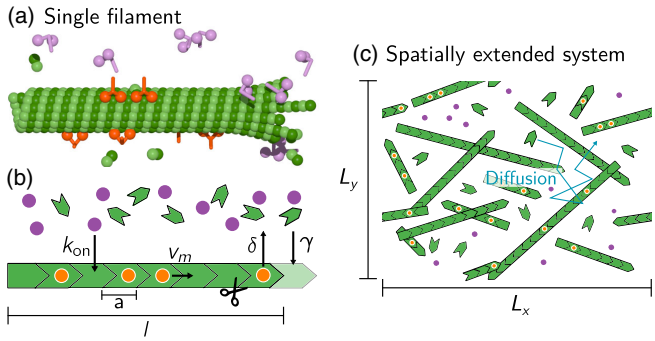


FIG. 1. Agent-based model. (a) Illustration of a filament interacting with a finite amount of tubulin (green) and motor proteins. Motors can be either cytosolic (purple) or filament-bound (orange). (b) Model representation of a single protofilament. (c) Illustration of a filament-motor mixture in a box geometry with periodic boundary conditions.

position $\mathbf{b}_i$ and fixed orientation $\theta_i \in [0, 2\pi)$, which are drawn randomly from uniform distributions. We have checked that diffusive motion of filaments does not affect the mechanism described here (see Supplemental Material Sec. IV [42] and movies 3–5) [42]. The lengths $l_i(t)$ of the individual filaments are dynamic variables that change by polymerization kinetics at the plus end. When filaments shrink to zero length, they are assumed to regrow from the same minus-end position and with the same orientation; filament shrinkage to zero length, though, rarely occurs. In the cytosol, both motors and tubulin units diffuse freely with diffusion constants $D_M$ and $D_T$, respectively. Cytosolic motors can bind with rate $k_{\mathrm{on}}$ to any point that is within the binding radius $r_M$ along a filament; for details see Supplemental Material Sec. SII [42]. Filament-bound motors move towards the filament plus end at speed $v_m$, where they catalyze filament depolymerization at rate $\delta$ [see Fig. 1(b)]. Upon depolymerization, the filament length is reduced by one tubulin unit (of length $a$) and both the plus-end-bound motor and the associated tubulin unit are released into the cytosol. As we consider stabilized microtubules no rapid depolymerization events upon microtubule catastrophes are considered here. Cytosolic tubulin within a distance $r_T$ of a filament plus end, binds to it at the rate $\gamma$, increasing filament length by $a$ [Fig. 1(d)]. We implicitly assume fast tubulin nucleotide exchange by allowing for immediate reattachment of tubulin. Finite nucleotide exchange does not qualitatively change the results (see Supplemental Material Sec. V) [42].

*Single-filament dynamics.*—Consider a cytosolic volume $V_0$, containing a single filament and a finite number of tubulin units $\rho_T V_0$ and motor proteins $\rho_M V_0$. For now, we assume for simplicity that the cytosolic concentrations $c_M$ and $c_T$ are spatially uniform; this assumption is relaxed when we discuss a spatially extended system with many filaments. The length change of the filament is determined by the antagonism between polymerization and depolymerization kinetics $\partial_t l(t) = v_g - v_s$ with the growth and shrinkage velocity given by $v_g = a c_T \gamma$ and $v_s = a m^+(t)\delta$, respectively, where $m^+(t)$ denotes the density of motors bound to the plus end [22,25].

For biologically relevant parameter ranges, the motor dynamics are fast compared to filament growth and shrinkage [10,26]. This separation of timescales implies that for a given filament length, the motor density can be assumed to be in a quasisteady state, where the total attachment flux of motors onto the filament, $j_{\mathrm{on}} = k_{\mathrm{on}} \tilde{c}_M l$, and the off-flux due to depolymerization events at the plus end, $j_{\mathrm{off}} = \tilde{v}_{\mathrm{s}}/a$, are in balance; quasisteady states are indicated by a tilde. Thus, the depolymerization velocity $\tilde{v}_{\mathrm{s}} = a k_{\mathrm{on}} l \tilde{c}_M$ is determined by the cytosolic density $\tilde{c}_M$, which in turn is related to the filament-bound motor number $\tilde{M}$ via mass conservation $\rho_M V_0 = \tilde{c}_M V_0 + \tilde{M}$. In steady state, the filament-bound motor density exhibits an antenna profile $\tilde{m}(s) = (k_{\mathrm{on}} \tilde{c}_M / v_m) s$ [60], which is inferred from the transport

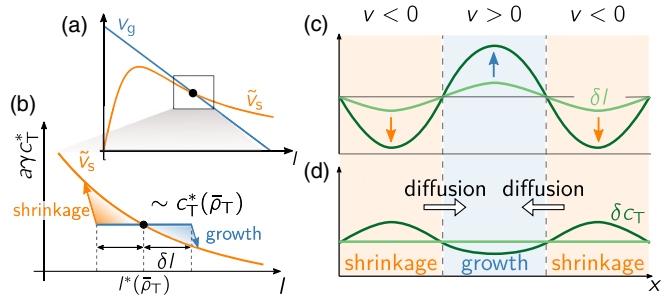


FIG. 2. (a) Shrinkage velocity $\tilde{v}_{\mathrm{s}}$ and growth velocity $v_g$ as a function of the filament length $l$ with the steady state length $l^*$ determined by the intersection point(s) of $v_g$ and $\tilde{v}_{\mathrm{s}}$. (b)–(d) Graphical analysis of the lateral instability.

equation $\partial_t m(s,t) = -v_m \partial_s m(s,t) + k_{\mathrm{on}} c_M(t)$ [43,44], implying $\tilde{M} = (k_{\mathrm{on}} \tilde{c}_M / 2v_m) l^2$. Combining the expression for the number of bound motors $\tilde{M}$ with mass conservation allows to express the shrinkage velocity in terms of the filament length and the total motor concentration $\rho_M$.

$$\tilde{v}_{\mathrm{s}}(l, \rho_M) = a k_{\mathrm{on}} l \tilde{c}_M = a k_{\mathrm{on}} l \frac{\rho_M}{1 + l^2/l_c^2}, \tag{1}$$

where we have defined the characteristic length scale $l_c := \sqrt{2 v_m V_0 / k_{\mathrm{on}}}$. For filament lengths $l < l_c$, the shrinkage velocity increases with the filament length, as would be expected with unlimited motor resources and has been observed experimentally [10,19]. At $l = l_c$ the number of cytosolic motors $c_M V_0$ equals the number of filament-bound motors $\tilde{M} = (k_{\mathrm{on}} \tilde{c}_M / 2v_m) l^2$. Increasing the filament length beyond $l_c$ leads to a depletion of the cytosolic motor pool and thereby a decreased on-flux $k_{\mathrm{on}} \tilde{c}_M l$. According to the flux balance condition, this reduces the off-flux $\tilde{v}_{\mathrm{s}}/a$ and thus the shrinkage velocity, so that $\tilde{v}_{\mathrm{s}} \sim 1/l$ for $l \gg l_c$ [see Fig. 2(a)].

The growth velocity $v_g$ can be written in terms of filament length $l$ and total tubulin density $\rho_T$ using tubulin mass conservation $(\rho_T V_0 = c_T V_0 + l/a)$ as $v_g(l, \rho_T) = \gamma(\rho_T a - l/V_0)$. At steady state the filament growth and shrinkage velocity are balanced, $v_g(l, \rho_T) = \tilde{v}_{\mathrm{s}}(l, \rho_M)$, which determines the steady state length $l^*(\rho_T, \rho_M)$ [Fig. 2(a)] [61].

*Self-organization in a spatially extended system.*—How does the length regulation of individual filaments play out in a spatially extended system where resources are shared by cytosolic diffusion between many filaments? In the limiting case where the cytosolic concentration is slowly varying on the scale of the (typical) filament length, the filaments can be treated as pointlike objects carrying a tubulin mass proportional to their length $l(\mathbf{x}, t)$. The single filament dynamics can then immediately be generalized to a local length regulation dynamics

$$\partial_t l(\mathbf{x}, t) = a\gamma c_T(\mathbf{x}, t) - \tilde{v}_{\mathrm{s}}(\mathbf{x}, t), \tag{2}$$

with the local shrinkage speed given in terms of the local quasisteady state approximation for the cytosolic motor density, $\tilde{v}_s(\mathbf{x},t)=ak_{on}l(\mathbf{x},t)\tilde{c}_M[l(\mathbf{x},t),\rho_M(\mathbf{x},t)]$ [cf. Eq. (1)]. The dynamics of the cytosolic tubulin concentration is governed by a reaction-diffusion equation

$$\partial_t c_T(\mathbf{x},t) = D_T\nabla^2 c_T(\mathbf{x},t) - \frac{\gamma c_T(\mathbf{x},t) - \tilde{v}_s(\mathbf{x},t)/a}{V_0}, \quad (3)$$

where the local polymerization kinetics induces sinks and sources of cytosolic tubulin; here $V_0 = V/N_F$ denotes the cytosolic volume associated with a single filament. The total motor density is redistributed by cytosolic diffusion

$$\partial_t \rho_M(\mathbf{x},t) = D_M\nabla^2\tilde{c}_M[l(\mathbf{x},t),\rho_M(\mathbf{x},t)], \quad (4)$$

where we again used the local quasi-steady state approximation for the cytosolic motor density $\tilde{c}_M(\mathbf{x},t)$. Taken together, Eqs. (2)–(4) form a closed set governing the system's dynamics in the long-wavelength limit.

The stability of a spatially uniform state $(l^*, c_T^*, \bar{\rho}_M)$ against spatial perturbations can be studied using a linear stability analysis (see Supplemental Material Sec. SIV for details [42]). Figure 3 shows a typical dispersion relation $\sigma(q)$ for the eigenvalue with the largest real part and the ensuing stability diagram as a function of $\bar{\rho}_M$ and $\bar{\rho}_T$. For $\bar{\rho}_T > \bar{\rho}_T^{\rm crit}(\bar{\rho}_M)$ there is a band of unstable Fourier modes $q \in (0, q_{\max})$ extending to long wavelengths ($q \to 0$). It is instructive to first consider the particular limit of well-mixed cytosolic tubulin. Then, the marginal mode $q_{\max}$ reduces to $q_{\max}^2 = -\rho_M\partial_l\tilde{v}_s|_{l^*}/(D_M\tilde{c}_M)$. This implies that there is an instability against spatial perturbations (lateral instability) only if $\partial_l\tilde{v}_s|_{l^*} < 0$. Moreover, the band of unstable modes narrows with increasing $D_M$, showing that cytosolic motor diffusion attenuates the lateral instability. Relaxing the assumption of well-mixed cytosolic tubulin, i.e., explicitly accounting for tubulin diffusion, yields the critical ratio of diffusion constants $D_T^{\rm crit}/D_M \approx \gamma/(ak_{on}V_0\bar{\rho}_M)$ in the limit $l^* \gg l_c$. For physiological parameters, we find that there is a lateral instability if the average number of motors per filament satisfies $\bar{\rho}_M^{\rm crit}V_0 > 0.57\ D_M/D_T$. This condition is well met for biologically relevant motor concentrations as $D_M/D_T \sim 1/6$ (see Supplemental Material Sec. SI [42]).

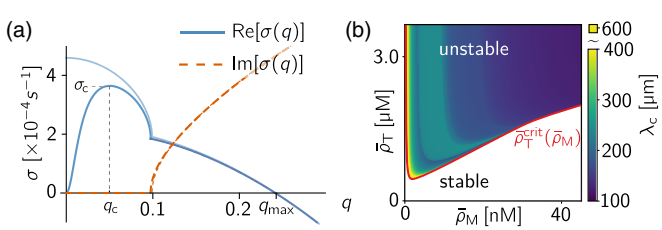


FIG. 3. (a) Leading eigenvalue in the dispersion relation $\sigma(q)$ for $\bar{\rho}_M = 50$ nM, $\bar{\rho}_T = 2.75$ μM, $D_M = 0.5\ \mu m^2\,s^{-1}$, and $D_T = 6\ \mu m^2\,s^{-1}$; other parameters are specified in the Supplemental Material Sec. SI [42]. The dispersion relation in the limit of well-mixed cytosolic tubulin is shown in light blue. (b) Stability diagram and wavelength of the fastest growing mode $q_c$ in the $(\bar{\rho}_M, \bar{\rho}_T)$-parameter space. The boundary of the laterally stable parameter regime, $\bar{\rho}_T^{\rm crit}(\bar{\rho}_M)$, is shown in red.

The feedback mechanism underlying the lateral instability can be explained in terms of a mass-redistribution instability [45,46,62]. To simplify the argument, we set $D_M = 0$ for the moment so that the total motor density remains invariant under the dynamics and therefore spatially uniform $\rho_M = \bar{\rho}_M$, cf. Eq. (4). Consider now a small perturbation $\delta l(\mathbf{x})$ added to the homogeneous state $l^*$, while keeping the cytosolic tubulin concentration $c_T(\mathbf{x}) = c_T^*$ initially constant [Figs. 2(b) and 2(c)]. Since then $v_g = a\gamma c_T$ initially remains uniform, the effect of $\delta l(\mathbf{x})$ on the net growth velocity $v = v_g - \tilde{v}_s$ depends on the slope of the shrinkage velocity at $l^*$. For $\partial_l\tilde{v}_s|_{l^*} < 0$, filaments grow (shrink) when they are long (short). This leads to an decrease (increase) of the cytosolic tubulin concentration [arrows in Figs. 2(b) and 2(c)] creating gradients in the cytosolic tubulin concentration that drive diffusive transport of tubulin mass towards regions of increased filament length. Since this tubulin mass redistribution leads to an increase of $v_g$ in regions where $\delta l > 0$, it promotes further filament growth there, i.e., the initial spatial perturbation $\delta l(\mathbf{x})$ is amplified [Fig. 2(b)]. In contrast, if the regulatory kinetics is such that the shrinkage velocity increases with filament length ($\partial_l\tilde{v}_s|_{l^*} > 0$), the effect is opposite. Cytosolic tubulin diffusion then redistributes the tubulin mass to regions with shorter filaments, counteracting the original disruption. Taken together, one finds the condition $\partial_l\tilde{v}_s|_{l^*} < 0$ for a spatial instability that is driven by free tubulin diffusion, in accordance with the result of the linear stability analysis.

The above reasoning also explains why cytosolic diffusion of motor proteins mitigates the lateral instability. Regions with short filaments contain fewer binding sites for motors and thus the cytosolic motor concentration is high there. The opposite holds for regions with long filaments. This creates gradients, and thereby diffusive fluxes, of motors towards regions of long filaments. The resulting diffusive influx of motors increases the rate of filament depolymerization there and thus counteracts the instability driven by tubulin diffusion.

*Agent-based simulations.*—To study the spatiotemporal dynamics above the critical tubulin concentration $\bar{\rho}_T^{\rm crit}(\bar{\rho}_M)$ we perform agent-based simulations. While Eqs. (2)–(4) capture well the initial dynamics at the long-wavelength instability, they fail to give the correct dynamics once gradients begin to emerge at the small length scales (see Supplemental Material Sec. SIV [42]). What this continuum theory lacks are effects due the spatial extent of the filaments which includes motor binding along the length of filaments as well as motion of each filament plus end due to polymerization kinetics.

Figure 4 shows a time sequence obtained from the simulations (see also movie 1 [42]). First, regions with

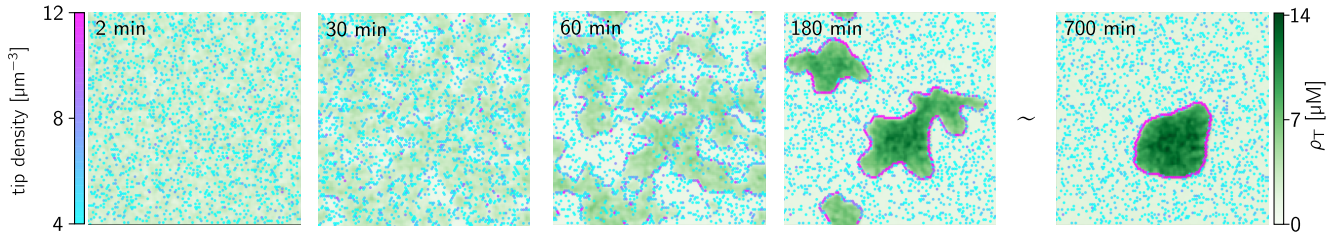


FIG. 4. Snapshots of the total tubulin density $\rho_T(\mathbf{x}, t)$ and the tip density. Parameters are as in Fig. 3(a); $L_x = L_y = 150$ μm.

short (depletion zones) and long (clusters) filaments are formed, which corresponds to the initial dynamics described by the mass redistribution instability (Fig. 4, $t = 30$ min). Moreover, filament plus ends start to accumulate at the interface between these zones. As the dynamics progresses, the depletion zones grow in size and the interfaces sharpen (Fig. 4, $t = 60$ min). At this time point, the filament-length distributions match on a qualitative level with experimental measurements [26] (see Supplemental Material Sec. SIII [42]). Subsequently, the high density regions segregate into individual large scale filament clusters, which are characterized by sharp boundaries and strong colocalization of filament plus ends at their periphery (Fig. 4, $t = 180$ min). This colocalization is caused by the movement of the filaments' plus end due to polymerization dynamics that is directed to zones where the net growth rate changes sign, namely, cluster interfaces. In the long run, the large filament clusters grow at the expense of the smaller ones, until eventually only a single cluster remains, which then develops into an asterlike structure (Fig. 4, $t = 700$ min).

Inside the clusters, the filaments exhibit net polar order that is aligned along tubulin-density gradients, i.e., orthogonal to the cluster boundaries. This is because the plus ends localized there belong predominantly to filaments whose minus end lies within the cluster's interior, implying an orientation orthogonal to the boundary on average (see Fig. 5, and movie 2 [42]).

To quantify this effect, we monitor the density gradient $\nabla\rho_T$, the local net polarity $\mathbf{p}$, and the angle $\theta$ enclosed between these vectors. Figure 5(d) shows the time evolution of the histogram $\mathcal{P}(\theta)$ of the angle $\theta$ weighted by the product of the magnitudes of $\nabla\rho_T$ and $\mathbf{p}$ to highlight the alignment of filaments near the cluster boundaries. The initially uniform distribution $\mathcal{P}(\theta)$ evolves quickly into a peaked distribution centered around zero—indicating the onset of polar order—and subsequently sharpens slowly; see also snapshots in insets of Fig. 5(a). The onset of this polar order occurs simultaneously with the mass-redistribution instability, as can be seen from the comparison of the spatial averages $\langle \mathbf{p} \cdot \nabla\rho_T \rangle$ and $\langle |\nabla\rho_T|^2 \rangle$, which are coarse-grained measures of filament orientation and density gradients, respectively; Fig. 5(e).

The polar order leads to advective flow of filament-bound motors out of clusters, which is balanced against diffusive influx caused by gradients in cytosolic motor concentration [see Fig. 5(c)]. Fast binding of motors inside clusters together with advective motor transport leads to the depletion of motors in the cluster interior and the formation of sharp gradients in cytosolic motor concentration. Those gradients help to maintain the filament plus-end localization at the interfaces: Plus ends that protrude beyond the interface are subjected to an increased on-flux of motors, causing the filaments to shrink back. Conversely, plus ends within the cluster are subjected to a reduced motor on-flux, causing them to grow towards the interface. Finally, the sharp cytosolic gradient leads to a shrinkage velocity $\tilde{v}_s$ that is independent of filament length because motor attachment occurs only in a narrow band at the interface. This is a collective effect and in contrast to the length regulation of a single filament, which is strongly length dependent [cf. Eq. (1)]. The size regulation of clusters and a quantitative analysis of the final, asterlike, stationary state will be presented in a forthcoming publication [63].

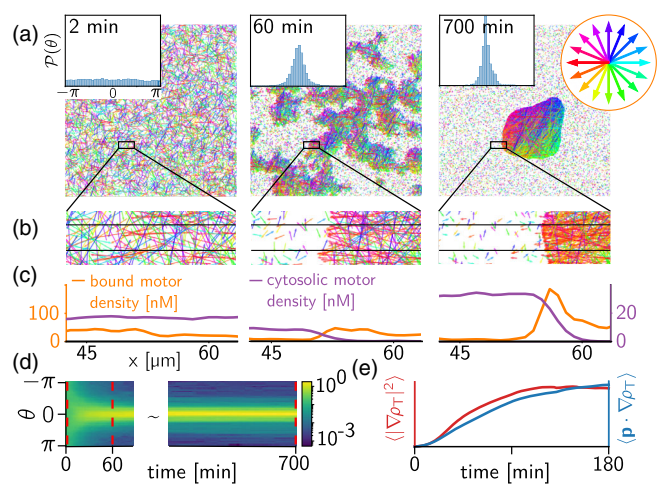


FIG. 5. (a) Snapshots of filament arrangement in Fig. 4. Filaments are color coded according to their orientation (color wheel); insets show the weighted distribution $\mathcal{P}(\theta)$. (b) Zoom into a structure interface. (c) Filament-bound (orange) and cytosolic (purple) motor concentration averaged along the vertical direction for the area enclosed by the black windows in (b). (d) Kymograph of $\mathcal{P}(\theta)$ with the (logarithmic) color scale showing the normalized (by area) frequency of the measured angles; the dashed, red lines correspond to the insets in (a). (e) Time trace of $\langle \mathbf{p} \cdot \nabla\rho_T \rangle$ and $\langle |\nabla\rho_T|^2 \rangle$ (ordinate in a.u.).

*Discussion.*—Commonly, the spatial self-organization of cytoskeletal filaments is attributed to motor proteins that reorient and move filaments by mechanical forces, such as dynein or kinesin-5 [7,18,64,65]. Here, we have shown that microtubule length regulation (through kinesin-8) in combination with resource limitation can lead to asterlike spatial patterns. The underlying instability is driven by diffusive redistribution of cytosolic tubulin mass. While we studied a minimal model for stabilized microtubules in an *in vitro* setting here, we expect that this instability mechanism could also operate in living cells or cell extracts. It has been estimated that up to 60% of the available tubulin heterodimers are used up during the formation of the mitotic spindle [66,67]. Moreover, length-dependent polymerization kinetics has been observed for nonstabilized microtubules [68]. Those observations—resource limitation and a length-dependent feedback mechanism—are the general requirements for the mass-redistribution instability discussed here. In general, we expect that the mechanism described here can play a role when tubulin as well as MAPs are limited. The pattern-forming instability we have discovered is also a potential candidate to explain the emergent self-organization observed in cell extracts [69]. Notably, this self-organization is heralded by spatial patterns that emerge in the tubulin density, which have comparable morphology and wavelength ($\sim 100\ \mu m$) as those we observe in our simulations (cf. Fig. 4). We also expect that our theory for resource-limited filament length regulation can be used to investigate heterogeneous growth dynamics in systems where spatial heterogeneities in filament length and/or density are imposed, e.g., by experimental design [39] or by upstream gradients [70,71]. From a broader perspective, the conceptual model investigated here is in itself an interesting active matter system exhibiting self-organized patterns, polarity sorting, and coarsening. Such collective filament organization is usually attributed to the mechanical interaction of filaments [17,72–75]. Investigating how mechanical interaction and length regulation work together will be an important starting point for further research.

We would like to thank Henrik Weyer, Isabella Graf, and Philipp Geiger for careful reading of the manuscript. We gratefully acknowledge the Deutsche Forschungsgemeinschaft (DFG, German Research Foundation) through the Excellence Cluster ORIGINS under Germany's Excellence Strategy (EXC-2094-390783311) and through the SFB863, Project No. 111166240.

*M. S. and F. B. contributed equally to this work.
†frey@lmu.de

[1] Eva Nogales, Structural insights into microtubule function, Annu. Rev. Biochem. **69**, 277 (2000).
[2] Daniel A. Fletcher and R. Dyche Mullins, Cell mechanics and the cytoskeleton, Nature (London) **463**, 485 (2010).
[3] Jonathon Howard, Mechanical signaling in networks of motor and cytoskeletal proteins, Annu. Rev. Biophys. **38**, 217 (2009).
[4] J. Howard, Molecular motors: Structural adaptations to cellular functions, Nature (London) **389**, 561 (1997).
[5] Robert A. Cross and A. McAinsh, Prime movers: The mechanochemistry of mitotic kinesins, Nat. Rev. Mol. Cell Biol. **15**, 257 (2014).
[6] Sabine Petry, Mechanisms of mitotic spindle assembly, Annu. Rev. Biochem. **85**, 659 (2016).
[7] Michael J. Shelley, The dynamics of microtubule/motor-protein assemblies in biology and physics, Annu. Rev. Fluid Mech. **48**, 487 (2016).
[8] Jonne Helenius, Gary Brouhard, Yannis Kalaidzidis, Stefan Diez, and Jonathon Howard, The depolymerizing kinesin MCAK uses lattice diffusion to rapidly target microtubule ends, Nature (London) **441**, 115 (2006).
[9] Gary J. Brouhard, Jeffrey H. Stear, Tim L. Noetzel, Jawdat Al-bassam, Kazuhisa Kinoshita, Stephen C. Harrison, Jonathon Howard, and Anthony A. Hyman, XMAP215 is a processive microtubule polymerase, Cell **132**, 79 (2008).
[10] Vladimir Varga, Cecile Leduc, Volker Bormuth, Stefan Diez, and Jonathon Howard, Kinesin-8 motors act cooperatively to mediate length-dependent microtubule depolymerization, Cell **138**, 1174 (2009).
[11] Jonathon Howard and Anthony A. Hyman, Microtubule polymerases and depolymerases, Curr. Opin. Cell Biol. **19**, 31 (2007).
[12] F. J. Ndlec, T. Surrey, and S. Leibler, Self-organization of microtubules and motors, Nature (London) **389**, 305 (1997).
[13] Thomas Surrey, François Nédélec, Stanislas Leibler, and Eric Karsenti, Physical properties determining self-organization of motors and microtubules, Science **292**, 1167 (2001).
[14] K. Kruse and F. Jülicher, Actively Contracting Bundles of Polar Filaments, Phys. Rev. Lett. **85**, 1778 (2000).
[15] K. Kruse, J. F. Joanny, F. Jülicher, J. Prost, and K. Sekimoto, Asters, Vortices, and Rotating Spirals in Active Gels of Polar Filaments, Phys. Rev. Lett. **92**, 078101 (2004).
[16] Tong Gao, Robert Blackwell, Matthew A. Glaser, M. D. Betterton, and Michael J. Shelley, Multiscale Polar Theory of Microtubule and Motor-Protein Assemblies, Phys. Rev. Lett. **114**, 048101 (2015).
[17] Peter J. Foster, Sebastian Fürthauer, Michael J. Shelley, and Daniel J. Needleman, Active contraction of microtubule networks, eLife **4**, e10837 (2015).
[18] Sebastian Fürthauer, Bezia Lemma, Peter J. Foster, Stephanie C. Ems-McClung, Che-Hang Yu, Claire E. Walczak, Zvonimir Dogic, Daniel J. Needleman, and Michael J. Shelley, Self-straining of actively crosslinked microtubule networks, Nat. Phys. **15**, 1295 (2019).
[19] V. Varga, J. Helenius, K. Tanaka, A. Hyman Anthony, U. Tomoyuki, Tanaka, and Howard Jonathon, Yeast kinesin-8 depolymerizes microtubules in a length-dependent manner, Nat. Cell Biol. **8**, 957 (2006).
[20] J. Helenius, G. Brouhard, Y. Kalaidzidis, S. Diez, and J. Howard, The depolymerizing kinesin MCAK uses lattice diffusion to rapidly target microtubule ends, Nature (London) **441**, 115 (2006).

[21] L. E. Hough, A. Schwabe, M. A. Glaser, J. R. McIntosh, and M. D. Betterton, Microtubule depolymerization by the kinesin-8 motor Kip3p: A mathematical model, Biophys. J. **96**, 3050 (2009).

[22] Louis Reese, Anna Melbinger, and Erwin Frey, Crowding of molecular motors determines microtubule depolymerization, Biophys. J. **101**, 2190 (2011).

[23] Anna Melbinger, Louis Reese, and Erwin Frey, Microtubule Length Regulation by Molecular Motors, Phys. Rev. Lett. **108**, 258104 (2012).

[24] Hui-Shun Kuan and M. D. Betterton, Biophysics of filament length regulation by molecular motors, Phys. Biol. **10**, 036004 (2013).

[25] Louis Reese, Anna Melbinger, and Erwin Frey, Molecular mechanisms for microtubule length regulation by kinesin-8 and XMAP215 proteins, Interface Focus **4**, 20140031 (2014).

[26] Matthias Rank, Aniruddha Mitra, Louis Reese, Stefan Diez, and Erwin Frey, Limited Resources Induce Bistability in Microtubule Length Regulation, Phys. Rev. Lett. **120**, 148101 (2018).

[27] K. Doubrovinski and K. Kruse, Self-Organization of Treadmilling Filaments, Phys. Rev. Lett. **99**, 228104 (2007).

[28] Nathan W. Goehring and Anthony A. Hyman, Organelle growth control through limiting pools of cytoplasmic components, Curr. Biol. **22**, R330 (2012).

[29] Keisuke Ishihara, Kirill S. Korolev, and Timothy J. Mitchison, Physical basis of large microtubule aster growth, eLife **5**, e19145 (2016).

[30] Göker Arpağ, Elizabeth J. Lawrence, Veronica J. Farmer, Sarah L. Hall, and Marija Zanic, Collective effects of XMAP215, EB1, CLASP2, and MCAK lead to robust microtubule treadmilling, Proc. Natl. Acad. Sci. U.S.A. **117**, 12847 (2020).

[31] Matthew C. Good, Michael D. Vahey, Arunan Skandarajah, Daniel A. Fletcher, and Rebecca Heald, Cytoplasmic volume modulates spindle size during embryogenesis, Science **342**, 856 (2013).

[32] James Hazel, Kaspars Krutkramelis, Paul Mooney, Miroslav Tomschik, Ken Gerow, John Oakey, and J. C. Gatlin, Changes in cytoplasmic volume are sufficient to drive spindle scaling, Science **342**, 853 (2013).

[33] Simone B. Reber, Johannes Baumgart, Per O. Widlund, Andrei Pozniakovsky, Jonathon Howard, Anthony A. Hyman, and Frank Jülicher, XMAP215 activity sets spindle length by controlling the total mass of spindle microtubules, Nat. Cell Biol. **15**, 1116 (2013).

[34] Ivana Gasic and Timothy J. Mitchison, ScienceDirect autoregulation and repair in microtubule homeostasis, Curr. Opin. Cell Biol. **56**, 80 (2019).

[35] Ana Milunović-Jevtić, Predrag Jevtić, Daniel L. Levy, and J. C. Gatlin, In vivo mitotic spindle scaling can be modulated by changing the levels of a single protein: The microtubule polymerase XMAP215, Mol. Biol. Cell **29**, 1311 (2018).

[36] Benjamin Lacroix, Gaëlle Letort, Laras Pitayu, Jérémy Sallé, Marine Stefanutti, Gilliane Maton, Anne Marie Ladouceur, Julie C. Canman, Paul S. Maddox *et al.*, Microtubule dynamics scale with cell size to set spindle length and assembly timing, Dev. Cell **45**, 496e6 (2018).

[37] Christopher Brownlee, Rebecca Heald, Christopher Brownlee, and Rebecca Heald, Importin a partitioning to the plasma membrane regulates intracellular scaling article importin a partitioning to the plasma membrane regulates intracellular scaling, Cell **176**, 805e8 (2019).

[38] Keisuke Ishihara, Franziska Decker, Paulo Caldas, James F. Pelletier, Martin Loose, Jan Brugués, and Timothy J. Mitchison, Spatial variation of microtubule depolymerization in large asters, Mol. Biol. Cell **32**, 869 (2021).

[39] Zachary M. Geisterfer, Daniel Y. Zhu, Timothy J. Mitchison, John Oakey, and Jesse C. Gatlin, Report microtubule growth rates are sensitive to global and local changes in microtubule plus-end density, Curr. Biol. **30**, 3016e3 (2020).

[40] A. Burakov, I. Vorobjev, I. Semenova, A. Cowan, J. Carson, Y. Wu, and V. Rodionov, Persistent growth of microtubules at low density, Mol. Biol. Cell **32**, 435 (2021).

[41] Ryoma Ohi, Claire Strothman, and Marija Zanic, Impact of the 'tubulin economy' on the formation and function of the microtubule cytoskeleton, Curr. Opin. Cell Biol. **68**, 81 (2021).

[42] See Supplemental Material at http://link.aps.org/supplemental/10.1103/PhysRevLett.129.238102 for movies 1–5 as well as technical background information, which includes Refs. [9,10,26,43–59].

[43] A. Parmeggiani, T. Franosch, and E. Frey, Phase Coexistence in Driven One-Dimensional Transport, Phys. Rev. Lett. **90**, 086601 (2003).

[44] A. Parmeggiani, T. Franosch, and E. Frey, Totally asymmetric simple exclusion process with Langmuir kinetics, Phys. Rev. E **70**, 046101 (2004).

[45] J. Halatek, F. Brauns, and E. Frey, Self-organization principles of intracellular pattern formation, Phil. Trans. R. Soc. B **373**, 20170107 (2018).

[46] Fridtjof Brauns, Jacob Halatek, and Erwin Frey, Phase-Space Geometry of Mass-Conserving Reaction-Diffusion Dynamics, Phys. Rev. X **10**, 041036 (2020).

[47] A. A. Hyman, D. Chrétien, I. Arnal, and R. H. Wade, Structural changes accompanying GTP hydrolysis in microtubules: Information from a slowly hydrolyzable analogue guanylyl-(alpha,beta)-methylene-diphosphonate, J. Cell Biol. **128**, 117 (1995).

[48] E. D. Salmon, W. M. Saxton, R. J. Leslie, M. L. Karow, and J. R. McIntosh, Diffusion coefficient of fluorescein-labeled tubulin in the cytoplasm of embryonic cells of a sea urchin: Video image analysis of fluorescence redistribution after photobleaching, J. Cell Biol. **99**, 2157 (1984).

[49] R. Schneider, T. Korten, W. J. Walter, and S. Diez, Kinesin-1 motors can circumvent permanent roadblocks by side-shifting to neighboring protofilaments, Biophys. J. **108**, 2249 (2015).

[50] Thomas D. Pollard, William C. Earnshaw, and Jennifer Lippincott-Schwartz, *Cell Biology*, 3rd ed. (Elsevier, Philadelphia, PA, 2017).

[51] Daniel T. Gillespie, Exact stochastic simulation of coupled chemical reactions, J. Phys. Chem. **81**, 2340 (1977).

[52] Reinhard Lipowsky, Stefan Klumpp, and Theo M. Nieuwenhuizen, Random Walks of Cytoskeletal Motors in Open and Closed Compartments, Phys. Rev. Lett. **87**, 108101 (2001).

[53] S. Klumpp and R. Lipowsky, Traffic of molecular motors through tube-like compartments, J. Stat. Phys. **113**, 233 (2003).

[54] P. S. Grassia, E. J. Hinch, and L. C. Nitsche, Computer simulations of Brownian motion of complex systems, J. Fluid Mech. **282**, 373 (1995).

[55] Franz Schwabl, *Statistical Mechanics*, 2nd ed. (Springer, New York, 2006).

[56] J. Tailleur and M. E. Cates, Statistical Mechanics of Interacting Run-and-Tumble Bacteria, Phys. Rev. Lett. **100**, 218103 (2008).

[57] T. Chou, K. Mallick, and R. K. P. Zia, Non-equilibrium statistical mechanics: from a paradigmatic model to biological transport, Rep. Prog. Phys. **74**, 116601 (2011).

[58] M. F. Carlier, R. Melki, D. Pantaloni, T. L. Hill, and Y. Chen, Synchronous oscillations in microtubule polymerization, Proc. Natl. Acad. Sci. U.S.A. **84**, 5257 (1987).

[59] R. Melki, M. F. Carlier, and D. Pantaloni, Oscillations in microtubule polymerization: The rate of GTP regeneration on tubulin controls the period, EMBO J. **7**, 2653 (1988).

[60] Note the occupation density of motors at the filament plus end is not equivalent to $\tilde{m}(l)$. The filament-bound motor density exhibits a boundary layer such that $v_m \tilde{m}(l) = am^+\delta$ [43,44].

[61] Depending on the functional form of the shrinkage velocity $\tilde{v}_s(l)$ the dynamics is either monostable with a single steady state length or bistable; see Supplemental Material Sec. SIV for details [42].

[62] J. Halatek and E. Frey, Phase-space geometry of mass-conserving reaction-diffusion dynamics, Nat. Phys. **14**, 507 (2018).

[63] Moritz Striebel, Fridtjof Brauns, and Erwin Frey, Filament bundle formation and polarity sorting through length regulation (unpublished).

[64] Ruensern Tan, Peter J. Foster, Daniel J. Needleman, and Richard J. McKenney, Cooperative accumulation of dynein-dynactin at microtubule minus-ends drives microtubule network reorganization, Dev. Cell **44**, 233e4 (2018).

[65] M. Striebel, I. Graf, and E. Frey, A mechanistic view of collective filament motion in active nematic networks, Biophys. J. **118**, 313 (2020).

[66] G. G. Borisy and E. W. Taylor, The mechanism of action of colchicine: Binding of colchincine-3H to cellular protein, J. Cell Biol. **34**, 525 (1967).

[67] G. G. Borisy and E. W. Taylor, The mechanism of action of colchicine: Colchicine binding to sea urchin eggs and the mitotic apparatus, J. Cell Biol. **34**, 535 (1967).

[68] Melissa K. Gardner, Marija Zanic, Christopher Gell, Volker Bormuth, and Jonathon Howard, Depolymerizing kinesins Kip3 and MCAK shape cellular microtubule architecture by differential control of catastrophe, Cell **147**, 1092 (2011).

[69] Xianrui Cheng and James E. Ferrell, Spontaneous emergence of cell-like organization in xenopus egg extracts, Science **366**, 631 (2019).

[70] Doogie Oh, Che-Hang Yu, and Daniel J. Needleman, Spatial organization of the ran pathway by microtubules in mitosis, Proc. Natl. Acad. Sci. U.S.A. **113**, 8729 (2016).

[71] Franziska Decker, David Oriola, Benjamin Dalton, and Jan Brugués, Autocatalytic microtubule nucleation determines the size and mass of spindles, eLife **7**, e31149 (2018).

[72] Julio M. Belmonte, Maria Leptin, and François Nédélec, A theory that predicts behaviors of disordered cytoskeletal networks, Mol. Syst. Biol. **13**, 941 (2017).

[73] Viktoria Wollrab, Julio M. Belmonte, Lucia Baldauf, Maria Leptin, François Nédélec, and Gijsje H. Koenderink, Polarity sorting drives remodeling of actin-myosin networks, J. Cell Sci. **132**, jcs219717 (2018).

[74] Jamie Rickman, François Nédélec, and Thomas Surrey, Effects of spatial dimensionality and steric interactions on microtubule-motor self-organization, Phys. Biol. **16**, 046004 (2019).

[75] Johanna Roostalu, Jamie Rickman, Claire Thomas, François Nédélec, and Thomas Surrey, Determinants of polar versus nematic organization in networks of dynamic microtubules and mitotic motors, Cell **175**, 796e14 (2018).